Research Repository UCD

Title	Pulsed Digital Oscillators for Electrostatic MEMS
Authors(s)	Fernandez, D., Jimenez, V., Madrenas, J., Gorreta, Sergi, Blokhina, Elena, Pons Nin, Joan, O'Connell, Diarmuid, Feely, Orla, Dominguez, Manuel
Publication date	2012-07-25
Publication information	Fernandez, D., V. Jimenez, J. Madrenas, Sergi Gorreta, Elena Blokhina, Joan Pons Nin, Diarmuid O'Connell, Orla Feely, and Manuel Dominguez. "Pulsed Digital Oscillators for Electrostatic MEMS" 59, no. 12 (July 25, 2012).
Publisher	IEEE
Item record/more information	http://hdl.handle.net/10197/3875
Publisher's statement	© 2012 IEEE. Personal use of this material is permitted. Permission from IEEE must be obtained for all other uses, in any current or future media, including reprinting/republishing this material for advertising or promotional purposes, creating new collective works, for resale or redistribution to servers or lists, or reuse of any copyrighted component of this work in other works.
Publisher's version (DOI)	10.1109/TCSI.2012.2206459

Downloaded 2024-04-17 22:05:51

The UCD community has made this article openly available. Please share how this access benefits you. Your story matters! (@ucd_oa)

© Some rights reserved. For more information

Pulsed Digital Oscillators for Electrostatic MEMS

S.Gorreta[1], D.Fernández[2], E.Blokhina[3], J.Pons-Nin[1], V.Jiménez[1], D. O'Connell[3], O.Feely[3], J.Madrenas[4], M.Domínguez[1*]

[1] Micro and Nano Technologies Group, [4] Advanced Hardware Architectures Group,
[1,4] Electronic Engineering Department, Universitat Politècnica de Catalunya, Spain
[2] Baolab Microsystems, Terrassa, Spain
[3] School of Electrical, Electronic and Communications Engineering, University College Dublin, Ireland
[*] corresponding author email: manuel.dominguez@upc.edu

***Abstract*—This paper introduces a new actuation scheme for implementing Pulsed Digital Oscillators (PDOs) for electrostatic MEMS resonators. In this scheme, the capacitance of the device is biased with a voltage and it is periodically sampled. Short pulses of zero voltage are applied depending on the decisions taken by the oscillator loop. The paper discusses in detail the implementation of such electrostatic PDO (e-PDO) through a prototype and links the e-PDO to the conventional PDO theory. As an example, it is shown that with this actuation scheme it is possible to excite different resonances of the mechanical structure simply by changing the parameters of the feedback filter of the oscillator.**

***Index Terms*—Microelectromechanical systems (MEMS), oscillators, electrostatic actuation**

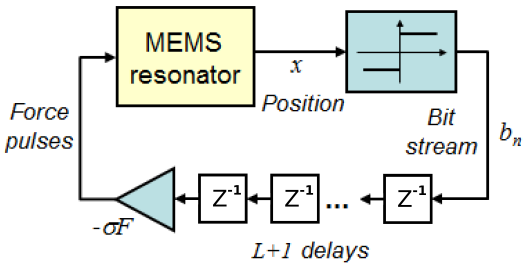

Figure 1. Standard PDO topology with a simple feedback loop, being $\sigma = \pm 1$ the sign and $L+1$ the number of delays.

I. Introduction

Resonant Microelectromechanical Systems (MEMS) are widely used in many areas (inertial sensors, chemical sensors, etc.) [1]–[5]. Specifically, some sensors detect small shifts of the resonant frequency of a mechanical structure as a result of changes in the variable to be measured. Some oscillator topologies have been proposed to work with MEMS resonators [6], [7]. Among them, Pulsed Digital Oscillators, PDOs, are a family of sigma-delta inspired circuit topologies designed to overcome some of the typical nonlinearities in MEMS sensing and actuation.

The aim of this paper is to present a new actuation scheme designed to implement Pulsed Digital Oscillators (PDOs) for electrostatic MEMS resonators. Until now, PDOs have been practically implemented with MEMS using thermoelectric actuation and piezoresistive position sensing [8], [9]. In this work we present a new actuation scheme allowing the adaptation of the PDO topology to the specific requirements of electrostatic MEMS. Due to a straightforward fabrication process, electrostatic actuators became very common and can be found in many applications [10], including cantilevers, switches, micromirrors, etc. The PDO topology implemented with electrostatic actuation and control electronics is simpler and cheaper to fabricate and it will offer the advantages of *smart sensor* technology [11].

Since this adaptation does not produce exactly a standard PDO feedback loop, we call this topology e-PDO. It will be shown, though, that with this actuation scheme the main characteristics of PDOs actuating MEMS resonators are still maintained, namely the selective activation of different resonant modes of the mechanical resonator.

The standard PDO architecture, depicted in Fig. 1, is relatively simple: it includes a MEMS resonator embedded in a feedback loop composed of a 1-bit quantizer and a variable number of delay blocks. The position of the MEMS is evaluated at each sampling time and, depending on whether it is above or below its rest position, short pulses of force are applied or not to the resonator. Since PDOs provide a built-in conversion to the digital domain, the oscillation frequency of the resonator can be easily monitored in real time [8], [9] simply by processing the sequence of bits, or bit stream b_n, extracted from the feedback loop.

There is a rigorous theoretical understanding of the dynamics of standard PDOs seen as non linear systems [12], [13]. It has been established that PDOs can work either above and below the Nyquist limit [8] and that, under some conditions, the bit streams b_n are the sign of a sampled sinusoid (S^3) at the resonant frequency of the resonator [12], which may provide asymptotically maximum energy transfer to the resonator. It has also been demonstrated recently that different resonant modes of the resonator can be selectively activated in real-time by simply changing the feedback loop parameters and/or the sampling frequency [9], [14]. All these properties have been demonstrated experimentally in PDO systems that use MEMS resonators which have thermoelectric actuation and piezoresistive position sensing.

As commented above, the purpose of this paper is to present a new actuation scheme adapted to electrostatic MEMS

resonators (e-PDO). To this effect, an application-specific integrated circuit (ASIC) allowing to measure the instantaneous capacitance of the electrostatic MEMS has been designed. A constant bias voltage is applied to the resonator, but short pulses of zero voltage are applied when the feedback loop of the e-PDO determines that a negative excitation must be applied to the resonator. This means that the excitation in this case consists of pulses of amplitudes $\{-F, 0\}$.

Section II of this paper introduces the structure of the devices used and the electrostatic actuation and sensing methods applied. Then, both continuous and discrete time models for such electrostatic topologies are developed and checked through simulations. Section III describes the actuation and sensing interface designed and implemented. Finally, Section IV depicts some experimental results illustrating how the general PDO theory and features extend to the electrostatic case. An example of selective excitation of three different spatial modes of a MEMS device is also included.

II. Dynamical Model for the Electrostatic PDO

Since the actuation scheme proposed in this paper, the e-PDO, is not exactly the one of a standard PDO, we will first obtain in this section the iterative map allowing the analysis and simulation of the proposed circuit topology.

A. Electrostatic Devices, Actuation and Sensing

The device to be considered is shown in Fig. 2(a). It consists of a parallel plate MEMS structure with voltage actuation. In the electrical domain, this structure can be modelled as two capacitors in series: a variable one corresponding to the variable air gap and a fixed one corresponding to the dielectric layer. Thus the capacitance associated with the variable air gap is $A\varepsilon_0/[g-x(t)]$ and the capacitance associated with the the dielectric layer is $A\varepsilon_0\varepsilon_d/d$ where A is the device area, g is the equilibrium gap value, d is the thickness of the dielectric, $x(t)$ is a deviation from the equilibrium at an applied voltage, ε_0 is the vacuum permittivity and ε_d is the relative permittivity of the dielectric layer. The total MEMS capacitance is

$$C(x) = \frac{\varepsilon_0\varepsilon_d A}{d + \varepsilon_d(g-x)} \tag{1}$$

Since the MEMS is voltage-driven, the electrostatic force applied to the moveable plate due to a voltage $V(t)$ can be easily calculated as

$$F_e(x,t) = \frac{1}{2}V^2(t)\frac{\partial}{\partial x}C(x) = \frac{\varepsilon_0\varepsilon_d^2 A}{2[d+\varepsilon_d(g-x(t))]^2}V^2(t) \tag{2}$$

Let us explain here the actuation principle shown in Fig. 2(b). Most of the time the MEMS is biased with a DC voltage V_{DC} below the pull-in value [10]. This implies a default or equilibrium position of the moveable plate $x_{eq} > 0$ when no pulses are applied. On the other hand, the actuation voltage is set to zero for short times $\Delta t \ll T_s$ when pulses must be applied (i.e. for each '1' in the bit stream). According to this, oscillations could be seen as small MEMS movements around x_{eq}.

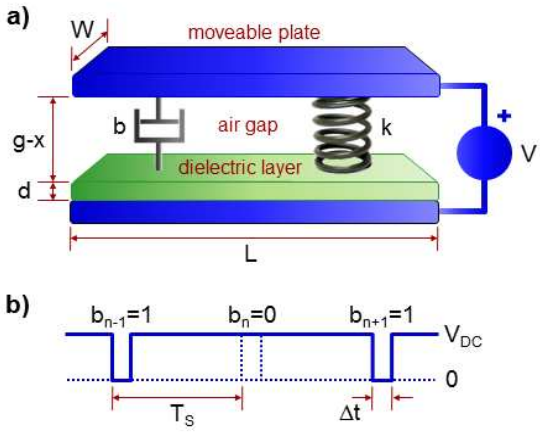

Figure 2. (a) Structure and main parameters of a voltage-driven parallel plate electrostatic MEMS; k is the spring factor, b the damping factor, d the width of the dielectric layer, x the position of the moveable plate and g the air gap when V=0. (b) Example of the MEMS actuation waveform after the bit stream $\{1,0,1\}$; $V = V_{DC}$ is the default bias, while $V = 0$ corresponds to force pulses. T_s is the sampling period and Δt the pulse width.

We can include this actuation mechanism in the expression of the electrostatic force, which can now be written as

$$F_e(x,t) = \frac{\varepsilon_0 A V_{DC}^2}{2[g_d - x(t)]^2}\left(1 - \sum_n b_{n-L}\Pi(t-nT_s)\right) \tag{3}$$

where $L+1$ is the number of delays in the e-PDO feedback loop, $\varepsilon = \varepsilon_0\varepsilon_d$, $g_d = g + d/\varepsilon_d$ and the function $\Pi(t)$ represents a square pulse of the form

$$\Pi(t) = \begin{cases} 1 & 0 < t < \Delta t \\ 0 & \text{otherwise} \end{cases} \tag{4}$$

The values of the e-PDO bit stream b_n are obtained at each sampling time through comparison of the current MEMS position x with time-averaged values x_{av_n} as follows

$$b_n = \frac{1}{2}(1 + \text{sgn}(x(nT_s) - x_{av_n})) \tag{5}$$

Note that the average values x_{av_n} and the equilibrium position x_{eq} introduced above may not be the same. For instance, x_{av_n} may be obtained in a practical implementation by low-pass filtering the position of the resonator:

$$x_{av_n} = \frac{(n-1)x_{av_{n-1}} + \frac{1}{T_s}\int_{(n-1)T_s}^{nT_s} x(t)dt}{n} \tag{6}$$

The position of the resonator x(t) has been obtained in our case by using a specific capacitance estimation circuit working in continuous time. This circuit is described in section III.

Once the MEMS device and the actuation and sensing principles are described, the objective now is to obtain a dynamical model that allows us to analyse the behaviour of the complete e-PDO system.

B. Continuous Time Model

The typical way to model the dynamics of MEMS structures as the one depicted in Fig.2(a) is through the following ordinary differential equation (ODE)

$$m\ddot{x}(t) + b\dot{x}(t) + kx(t) = F_e(x,t) \tag{7}$$

where m is the mass of the resonator, b is the damping coefficient, k is the spring constant and $F_e(x,t)$ is the electrostatic force applied to the moveable plate. The dot over the variable x denotes the time derivative.

Let us now normalise the position of the resonator as $y(t) = x(t)/g_d$. Note that we will restrict to the maximum value of $y(t)$ equal to $1/3$ that corresponds to the pull-in instability threshold [10]. After this change and using equation (3), the ODE (7) becomes

$$\ddot{y} + 2\gamma\dot{y} + \omega_0^2 y = \frac{K_0 V_{DC}^2}{(1-y)^2}\left(1 - \sum_n b_{n-L}\Pi(t - nT_s)\right) \tag{8}$$

where $\gamma = b/(2m)$ is the normalised dissipation parameter due to damping losses, $\omega_0 = \sqrt{k/m}$ is the natural frequency of the resonator and $K_0 = \varepsilon_0 A/(2mg_d^3)$ is the normalised coefficient that contains the applied voltage and the geometry parameters. Taking into account that, depending on the values of the bit stream, the voltage applied can be either $V = V_{DC}$ or $V = 0$, let us split the ODE into two different cases

$$\ddot{y} + 2\gamma\dot{y} + \omega_0^2 y = \begin{cases} 0 & \text{for} \quad V = 0 \\ \frac{K_0 V_{DC}^2}{(1-y)^2} & \text{for} \quad V = V_{DC} \end{cases} \tag{9}$$

Since most of time the resonator is subjected to the bias voltage $V = V_{DC}$, its dynamics may be seen as small signal-like movements around the equilibrium position y_{eq} caused by V_{DC}. The equilibrium position can be easily calculated as the only solution with physical meaning of the following third order equation

$$\omega_0^2 y_{eq} = \frac{K_0 V_{DC}^2}{(1-y_{eq})^2} \tag{10}$$

The linearisation of equation (9) around y_{eq} for the case $V = V_{DC}$, yields

$$\ddot{y} + 2\gamma\dot{y} + \omega_0^2 y = \frac{K_0 V_{DC}^2}{(1-y_{eq})^2} + \frac{2K_0 V_{DC}^2}{(1-y_{eq})^3}(y - y_{eq}) \tag{11}$$

Summarizing the above for the quasi-equilibrium case considered and merging expressions (10) and (11), equations (9) can now be written as

$$\ddot{y} + 2\gamma\dot{y} + \omega_0^2 y = 0 \quad \text{for} \quad V = 0 \tag{12}$$

$$\ddot{y} + 2\gamma\dot{y} + \omega_1^2 (y - y_{eq}) = 0 \quad \text{for} \quad V = V_{DC} \tag{13}$$

where

$$\omega_1^2 = \omega_0^2\left(1 - \frac{2y_{eq}}{1-y_{eq}}\right) \tag{14}$$

is the natural frequency of the MEMS when a constant bias voltage V is being applied. Let us also note that this model displays an anticipated effect: the natural frequency departs from ω_0 for $V \neq 0$. However, ω_1 is defined only for the range $0 \leq y_{eq} < 1/3$, i.e. for equilibrium positions below pull-in.

Finally, in order to specify the evolution of the MEMS position and velocity with time, let us write down a solution of equations (12) and (13) in matrix format for $V = 0$

$$\begin{pmatrix} y(t+\tau) \\ v(t+\tau) \end{pmatrix} = e^{-\gamma\tau} M_0(\tau) \begin{pmatrix} y(t) \\ v(t) \end{pmatrix} \tag{15}$$

and for $V = V_{DC}$

$$\begin{pmatrix} y(t+\tau) - y_{eq} \\ v(t+\tau) \end{pmatrix} = e^{-\gamma\tau} M_1(\tau) \begin{pmatrix} y(t) - y_{eq} \\ v(t) \end{pmatrix} \tag{16}$$

where τ is an arbitrary time lapse starting from the moment t. In the above expressions we have introduced the matrix $M(\tau)$

$$M_i(\tau) = \begin{pmatrix} a_{i_{11}}(\tau) & a_{i_{12}}(\tau) \\ a_{i_{21}}(\tau) & a_{i_{22}}(\tau) \end{pmatrix}, \qquad i = 0, 1 \tag{17}$$

and its components are

$$a_{i_{11}} = \cos(\tau\sqrt{\omega_i^2 - \gamma^2}) + \frac{\gamma}{\sqrt{\omega_i^2 - \gamma^2}}\sin(\tau\sqrt{\omega_i^2 - \gamma^2})$$

$$a_{i_{12}} = \frac{1}{\sqrt{\omega_i^2 - \gamma^2}}\sin(\tau\sqrt{\omega_i^2 - \gamma^2})$$

$$a_{i_{21}} = \frac{-\omega_i^2}{\sqrt{\omega_i^2 - \gamma^2}}\sin(\tau\sqrt{\omega_i^2 - \gamma^2})$$

$$a_{i_{22}} = \cos(\tau\sqrt{\omega_i^2 - \gamma^2}) - \frac{\gamma}{\sqrt{\omega_i^2 - \gamma^2}}\sin(\tau\sqrt{\omega_i^2 - \gamma^2})$$

It is convenient to introduce now normalized rotation matrices by employing the following transformation

$$M_i(t) = A_i^{-1} R_i(t) A_i \qquad i = 0, 1 \tag{18}$$

where the matrices A_i are defined as follows

$$A_i = \begin{pmatrix} 1 & 0 \\ \gamma/\sqrt{\omega_i^2 - \gamma^2} & 1/\sqrt{\omega_i^2 - \gamma^2} \end{pmatrix} \tag{19}$$

and the matrices R_i are the standard rotation matrices

$$R_i(t) = \begin{pmatrix} \cos(t\sqrt{\omega_i^2 - \gamma^2}) & \sin(t\sqrt{\omega_i^2 - \gamma^2}) \\ -\sin(t\sqrt{\omega_i^2 - \gamma^2}) & \cos(t\sqrt{\omega_i^2 - \gamma^2}) \end{pmatrix} \tag{20}$$

The velocity axis is also normalised using the matrix A_1

$$\begin{pmatrix} y(t) \\ \vartheta(t) \end{pmatrix} = A_1 \begin{pmatrix} y(t) \\ v(t) \end{pmatrix} \tag{21}$$

After these transformations, the evolution of the system in time can be written for $V = 0$ as

$$\begin{pmatrix} y(t+\tau) \\ \vartheta(t+\tau) \end{pmatrix} = e^{-\gamma\tau} A_1 A_0^{-1} R_0(\tau) A_0 A_1^{-1} \begin{pmatrix} y(t) \\ \vartheta(t) \end{pmatrix} \tag{22}$$

and for $V = V_{DC}$ as

$$\begin{pmatrix} y(t+\tau) - y_{eq} \\ \vartheta(t+\tau) \end{pmatrix} = e^{-\gamma\tau} R_1(\tau) \begin{pmatrix} y(t) - y_{eq} \\ \vartheta(t) \end{pmatrix} \tag{23}$$

C. Discrete-Time Model

Once the system of ODEs that models the temporal evolution of the electrostatic PDO has been obtained, the next step is to obtain a discrete-time model. It will allow the study of the system dynamics through iterative maps. If we define the set $\mathcal{B}$ as $\{1, -1\}$, the e-PDO map can be defined as follows

$$\mathbb{R}^3 \times \mathcal{B}^L \xrightarrow{T} \mathbb{R}^3 \times \mathcal{B}^L$$

$$(y_n, \vartheta_n, y_{av_n}, b_1, ..., b_L) \rightarrow$$
$$\rightarrow (y_{n+1}, \vartheta_{n+1}, y_{av_{n+1}}, \text{sgn}(y_n - y_{av}), b_1, ..., b_{L-1})$$

Let us introduce the following contraction coefficients: $\alpha = \exp(-\gamma T_s)$ and $\alpha_\delta = \exp(-\gamma \delta T_s)$, where δ is the normalised pulse width $\delta = \Delta t / T_s$. By denoting the identity matrix as I, the iterative map can be written as the following equation in the case if $b_L = -1$:

$$\begin{pmatrix} y_{n+1} \\ \vartheta_{n+1} \end{pmatrix} = \alpha R_1(T_s) \begin{pmatrix} y_n \\ \vartheta_n \end{pmatrix} + [I - \alpha R_1(T_s)] A_1 \begin{pmatrix} y_{eq} \\ 0 \end{pmatrix} \quad (24)$$

and as the following one in the case if $b_L = 1$

$$\begin{pmatrix} y_{n+1} \\ \vartheta_{n+1} \end{pmatrix} = \alpha R_1((1-\delta)T_s) A_1 A_0^{-1} R_0(\delta T_s) A_0 A_1^{-1} \begin{pmatrix} y_n \\ \vartheta_n \end{pmatrix} +$$
$$+ [I - (\alpha/\alpha_\delta) R_1((1-\delta)T_s)] A_1 \begin{pmatrix} y_{eq} \\ 0 \end{pmatrix} \quad (25)$$

If $L = 0$ then the previous assignment depends on the value of $\text{sgn}(y_n - y_{av_n})$.

Now, although in order to evaluate the map it is only necessary to evaluate the time evolution of the average value of the MEMS position, $y_{av_{n+1}}$, we will also obtain the corresponding values of the velocity, $\vartheta_{av_{n+1}}$. Thus, if we take into account that $y_{av} = x_{av}/g_d$ and according to equation (6), this evolution can be written for the $b_L = -1$ case as

$$\begin{pmatrix} y_{av_{n+1}} \\ \vartheta_{av_{n+1}} \end{pmatrix} = \frac{1}{n} \Bigg[(n-1) \begin{pmatrix} y_{av_n} \\ \vartheta_{av_n} \end{pmatrix} +$$
$$+ \frac{1}{T_s} \int_0^{T_s} e^{-\gamma t} R_1(t) dt \begin{pmatrix} y_n \\ \vartheta_n \end{pmatrix} +$$
$$+ \left(I - \frac{1}{T_s} \int_0^{T_s} e^{-\gamma t} R_1(t) dt \right) A_1 \begin{pmatrix} y_{eq} \\ 0 \end{pmatrix} \Bigg] \quad (26)$$

However, for the case $b_L = 1$ the integration interval splits into two time segments: a first one when $V = 0$ of width Δt, and the rest of the sampling period. Then the evolution for the $b_L = 1$ case can be written as the following system

$$\Delta_n^1 = A_1 A_0^{-1} \int_0^{\delta T_s} e^{-\gamma t} R_0(t) dt \cdot A_0 A_1^{-1} \begin{pmatrix} y(nT_s) \\ \vartheta(nT_s) \end{pmatrix} \quad (27)$$

$$\Delta_n^2 = \int_{\delta T_s}^{T_s} e^{-\gamma t} R_1(t) dt \begin{pmatrix} y((n+\delta)T_s) \\ \vartheta((n+\delta)T_s) \end{pmatrix} +$$
$$+ \left((1-\delta)T_s \cdot I - \int_{\delta T_s}^{T_s} e^{-\gamma t} R_1(t) dt \right) A_1 \begin{pmatrix} y_{eq} \\ 0 \end{pmatrix} \quad (28)$$

where

$$\begin{pmatrix} y((n+\delta)T_s) \\ \vartheta((n+\delta)T_s) \end{pmatrix} = \alpha_\delta A_1 A_0^{-1} R_0(\delta T_s) A_0 A_1^{-1} \begin{pmatrix} y(nT_s) \\ \vartheta(nT_s) \end{pmatrix} \quad (29)$$

Finally,

$$\begin{pmatrix} y_{av_{n+1}} \\ \vartheta_{av_{n+1}} \end{pmatrix} = \frac{1}{n} \left[(n-1) \begin{pmatrix} y_{av_n} \\ \vartheta_{av_n} \end{pmatrix} + \frac{1}{T_s} (\Delta_n^1 + \Delta_n^2) \right] \quad (30)$$

D. Connection with the standard PDO topology

Once we have found a discrete time model explaining the evolution of the e-PDO, let us analyze under what conditions it can be simplified to the standard equation governing a PDO, namely:

$$\begin{pmatrix} y_{n+1} \\ v_{n+1} \end{pmatrix} = e^{-\gamma T_S} M_1(T_S) \begin{pmatrix} y_n \\ v_n \end{pmatrix} - \begin{pmatrix} 0 \\ b_{n-L} \end{pmatrix} \quad (31)$$

where $b_{n-L} = 1/2(1 + \sigma sgn(y((n-L)T_S)))$. This means that the excitation of the PDO is always attractive, and therefore always takes zero or positive values. The advantage of this analysis is that it justifies to predict the behaviour of the e-PDO from the simple design rules of PDOs, therefore providing guidelines for the design and implementation of this new kind of systems.

Considering that the position of the resonator is near y_{eq} for some bias voltage V_{DC}, if we apply a different voltage $V + V_{DC}$ we obtain

$$\begin{pmatrix} y(t+\tau) - y_{eq} \\ v(t+\tau) \end{pmatrix} = e^{-\gamma\tau} M_x(\tau) \begin{pmatrix} y(t) - y_{eq} \\ v(t) \end{pmatrix} +$$
$$+ \begin{pmatrix} \frac{K_0 V}{\omega_x^2 (1-y_{eq})^2} (2V_{DC} + V)(1 - e^{-\gamma\tau} a_{x_{11}}) \\ -\frac{K_0 V}{\omega_x^2 (1-y_{eq})^2} (2V_{DC} + V) e^{-\gamma\tau} a_{x_{21}} \end{pmatrix} \quad (32)$$

where $M_x(\tau)$ is the usual rotation of the resonator but depending on w_x, defined as $\omega_x^2 = \omega_0^2 (1 - \frac{2y_{eq}}{1-y_{eq}} (1 + V/V_{DC})^2)$. Now, taking the limit of the pulse to obtain a delta, i.e. $\tau \rightarrow 0$ and $\tau V^2 \rightarrow F$ we have that:

$$\begin{pmatrix} y(t^+) - y_{eq} \\ v(t^+) \end{pmatrix} = \lim_{\tau \rightarrow 0, V^2\tau \rightarrow F} \Bigg[e^{-\gamma\tau} M_x(\tau) \begin{pmatrix} y(t) - y_{eq} \\ v(t) \end{pmatrix} +$$
$$+ \begin{pmatrix} \frac{K_0 V}{\omega_\delta^2 (1-y_{eq})^2} (2V_{DC} + V)(1 - e^{-\gamma\tau} a_{\delta_{11}}) \\ -\frac{K_0 V}{\omega_\delta^2 (1-y_{eq})^2} (2V_{DC} + V) e^{-\gamma\tau} a_{\delta_{21}} \end{pmatrix} \Bigg] =$$
$$= \begin{pmatrix} 1 & 0 \\ \frac{F}{V_{DC}^2} (\omega_0^2 - \omega_1^2) & 1 \end{pmatrix} \begin{pmatrix} y(t) - y_{eq} \\ v(t) \end{pmatrix} + \begin{pmatrix} 0 \\ \frac{F}{V_{DC}^2} \omega_0^2 y_{eq} \end{pmatrix} \quad (33)$$

Finally, considering that $\frac{y(t) - y_{eq}}{1 - y_{eq}} \ll 1/2$, which is the same as saying that we have a combination of F and γ providing sufficiently small displacements, we have that $(\omega_0^2 - \omega_1^2) \ll \omega_0^2 y_{eq}$. Then, the effect of applying a large voltage pulse would be approximately adding a constant to the instantaneous velocity of the resonator, threfore allowing us to obtain the standard equation of the PDO (31).

E. Simulation Results

Using the theoretical description of the system obtained in the previous sections, we have performed a set of MATLAB simulations in order to both validate the discrete time model and analyse the behaviour of e-PDO systems. The dashed line of fig. 3 shows a solution of the non linear ODE (8). There is a start-up transient of about 10 ms before the MEMS reaches the 'steady state' regime, with the self-sustained sinusoidal oscillations shown in fig. 3. Note that the MEMS position is always below $1/3$ of the normalized gap.

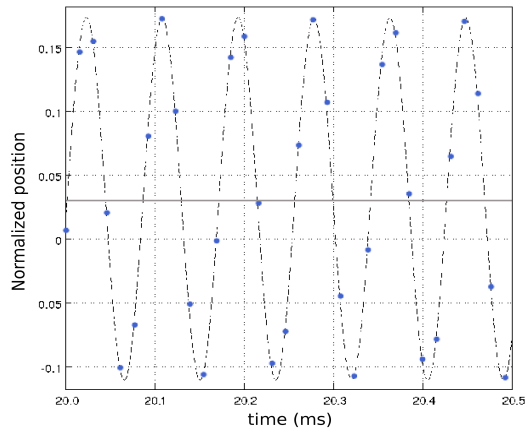

Figure 3. Simulation results showing the ODE (dashed line) and the iterative map (circles) solutions for the "steady-state" regime reached at $f_0 = 12.151\ kHz$, $f_s = 65\ kHz$, $\gamma = 381.7\,rad/s$ and $\delta = 7\%$. The continuous line is the position average y_{av}.

However, e-PDOs are nonlinear systems while the obtained iterative map described through (24) and (25) represents a model obtained by applying the linearisation (11). Therefore, the next objective is to validate the map through comparisons between continuous and discrete-time simulations. Fig. 3 also shows the steady state regime reached for both discrete (circles) and continuous (dashed line) time simulations. As is seen from this comparison, the map models the original continuous time system very well. Therefore, the simulations support our approach for obtaining the map.

On the other hand, Fig. 3 also shows that the normalized position average obtained through equations (26) and (30) has an almost constant value ($y_{av} = 0.03$), and this is an expected result since we observe sinusoidal oscillations. Let us remark that the average of the position is a key value, since it is the threshold in the e-PDO loop decisions (equation (5)).

The discrete-time simulation results depicted in fig. 4, obtained from equations (24) and (25) with the same parameters

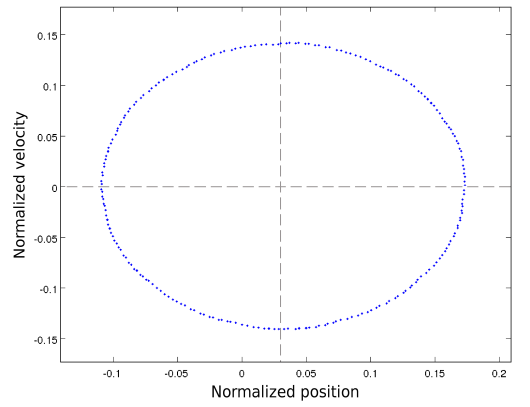

Figure 4. Phase space simulation of the discrete-time model corresponding to the same case as in fig. 3.

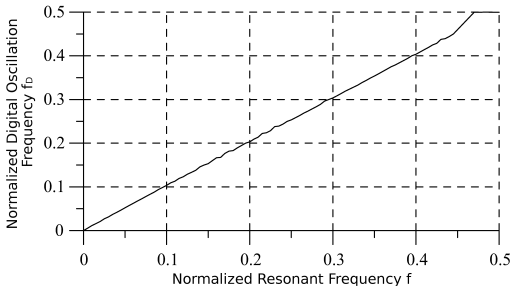

Figure 5. Digital frequency of oscillations f_D as a function of the normalised frequency $f = f_1/f_s$, $L = 0$ and $\rho = \gamma/\omega_0 = 0.001$.

as in fig. 3, show an example of the evolution of the e-PDO in the state space: a stable trajectory is reached.

Finally, we note that for resonant sensors the frequency of oscillations is a parameter of interest. For the conventional PDO topology the frequency can be directly calculated from the output bit stream. For PDOs not working beyond the Nyquist limit, the resulting oscillation frequency is $f_{osc} = f_s f_D$, where f_D is the digital frequency extracted from the bit stream. The same is applicable to the electrostatic PDO. We will use the route suggested in [12] to generate an auxiliary sequence and to obtain the digital frequency of oscillations f_D. The sequence is defined as follows

$$d_n = \begin{cases} 1 & \text{if } b_n \neq b_{n+1} \\ 0 & \text{if } b_n = b_{n+1} \end{cases} \tag{34}$$

If b_n is a perfect S^3 sequence, this conversion generates a 1st order $\Sigma\Delta$ (sigma-delta) sequence. The digital frequency of oscillations can now be written as

$$f_D = \frac{1}{2N} \cdot \sum_{n=1}^{N} d_n \tag{35}$$

where N is a large enough integer number. A fragment of the dependence of the digital frequency f_D on the normalised frequency $f = f_1/f_s$ where $2\pi f_1 = \omega_1$ from (14) is shown in fig. 5.

III. Experimental Setup

A. Overview

Once we successfully analysed the e-PDO from the theoretical point of view and verified its behaviour through simulations, now the objective is to experimentally validate the performance of such system with specific electrostatic MEMS resonators using the excitation and sensing mechanisms described in this section. The second but not the least objective is to validate if e-PDOs can be used to selectively excite different vibration modes of the MEMS resonator.

The implementation and operation of the e-PDO systems developed for carrying out the experimental work are similar to those used in other previous works, although in this case electrostatic MEMS resonators are used for the first time and this entails some significant differences and new properties concerning actuation, sensing and global behaviour.

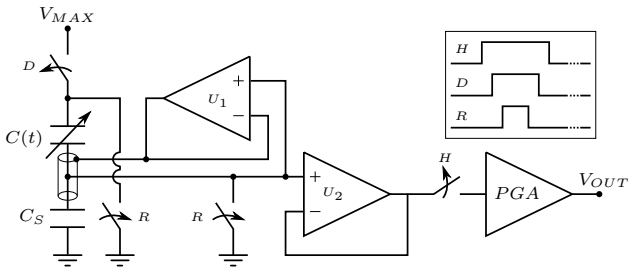

Figure 6. Simplified schematic of the electrostatic actuation and sensing interface. Note the active shielding on the intermediate node of the capacitive divider. The inset on the up-right corner shows the behaviour of control signals D, R and H

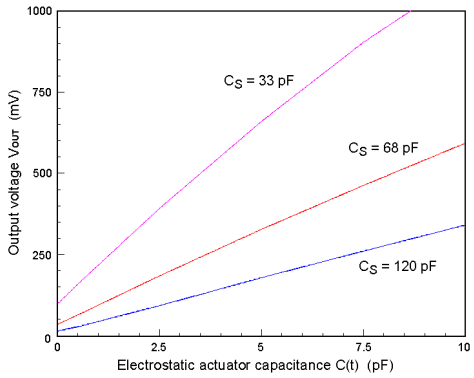

Figure 7. Simulation of the output voltage V_{OUT} vs. the electrostatic actuator capacitance $C(t)$ for three different C_S values (33 pF, 68 pF and 120 pF). V_{MAX} was set to 4.5 V and the PGA to a unity gain.

The e-PDO circuitry consists of analog and digital parts. The core component of the analog block is an ASIC that interfaces the MEMS with the rest of the system. Thus, it multiplexes in time the voltage actuation and capacitance sensing tasks. Design and operation of the analog part are described in the next section.

As in other previous works [8], [9], the e-PDO digital feedback loop has been implemented on an FPGA. In this way, the configuration of the main parameters of the e-PDO architecture, namely the sampling frequency T_s, the pulse width Δt, the number of delays L and the sign of the feedback loop, can be done easily in real-time.

Finally, it should be recalled here that, for a given MEMS resonator and sampling frequency, specific configurations of the digital loop allow to selectively excite different mechanical resonances of the MEMS, as shown in [9], [14].

B. Electrostatic Actuation and Sensing Interface

A simplified schematic of the electrostatic actuation and sensing interface [15] is depicted in fig. 6. Its architecture is based on detecting the voltage drop across a capacitive divider formed by the MEMS internal capacitance and a fixed capacitor. The electrostatic MEMS is represented as the variable capacitor $C(t)$, the maximum voltage applied to the MEMS is represented as V_{MAX} and the output voltage as V_{OUT}. C_S is a series capacitor and D (*Disconnect*), R (*Reset*), H (*Hold*) are digital signals controlling a set of CMOS switches. U_1 and U_2 are OpAmp-based voltage followers intended to provide cancellation of the parasitic capacitance and electrical isolation, respectively. A programmable-gain amplifier (PGA) provides up to 40 dB gain to the detected signal.

In sensing mode, signals R, D and H are all zero, thus the AC voltage at the middle of the capacitive divider formed by the electrostatic actuator $C(t)$ and the series capacitance C_S is given by the following expression,

$$V_{CS}(t) = V_{MAX}\frac{C(t)}{C_S + C(t)} \tag{36}$$

Provided that $C_S \gg C(t)$, the previous equation can be approximated to

$$V_{CS}(t) \approx C(t)\frac{V_{MAX}}{C_S} \tag{37}$$

From this, the intermediate node of the capacitive divider has a voltage approximately proportional to the actuator capacitance. However, this node has an infinite impedance at DC, which implies that no long-term stability of the measure can be guaranteed [16]. In fact, any leakage current flowing though the intermediate node of the capacitive divider will change the charge distribution between the capacitors and so the $V_{CS}(t)$ voltage, invalidating the measurement.

In order to solve this issue and, at the same time, generate the pulsed actuation signal required by the e-PDO, signals R and D are briefly set to one. This has the effect of disconnecting the MEMS from V_{MAX} and discharging the capacitors. When R and D are set to zero again, the charge in the capacitive divider is refreshed, thus the leakage phenomena do not compromise the measurement and long-term DC stability can be guaranteed [17], [18]. The purpose of signal H is to prevent the reset pulse to be propagated to the output through the amplification chain. For this, H is set to one before R or D are one and it is set to zero only when R and D are zero. The whole sequence of R, D and H pulses is called the reset sequence and it is controlled by a single ASIC pin.

In order to detect even small capacitance changes and to be able to measure MEMS actuators connected through a probe station setup, means of cancelling the effect of parasitic capacitances have to be provided. These parasitic capacitances, if grounded, are in parallel with C_S and increase its value, so attenuating the detected signal and limiting the minimum capacitance that can be measured. Operational amplifier U_1 allows cancellation of the parasitic capacitances by copying the V_{CS} voltage of the capacitive divider to the shielding of that connection, thus cancelling any voltage difference between V_{CS} and any parasitic node, and thereby, nulling the effect of parasitic capacitances. Precautions have to be taken to ensure the high-frequency stability of the loop when the measurement setup has large parasitic capacitances.

Figure 7 shows the simulation of the output voltage V_{OUT} for different values of the electrostatic actuator capacitance $C(t)$. Series capacitance was set to three different values: 33 pF, 68 pF (as used in the measurements) and 120 pF; the actuation voltage V_{MAX} to 4.5 V and the gain of the PGA to

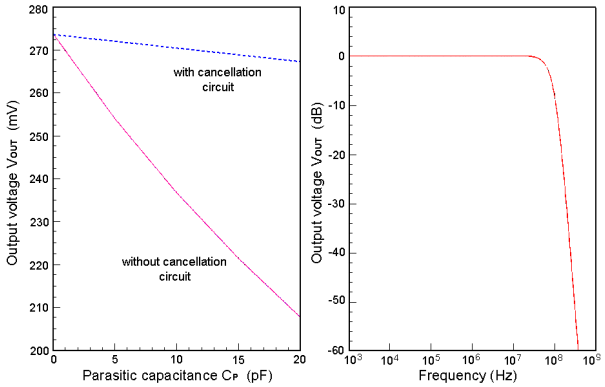

Figure 8. Left: simulation of the output voltage V_{OUT} vs. parasitic capacitance C_P with and without the parasitic-cancellation circuit. Right: frequency response of the capacitance estimator. C_S was set to 68 pF and V_{MAX} to 4.5 V.

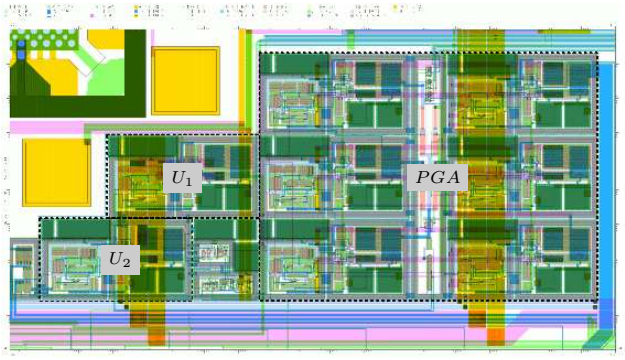

Figure 9. Layout of the electrostatic actuation and sensing interface. Voltage followers U_1 and U_2 and the programmable-gain amplifier (PGA) are shown. The circuit block between U_2 and the PGA contains the switches R, D and H and the charge-injection mitigation circuits. Shown area is 530 $\times$ 280 μm^2.

unity. In the simulation, the parasitic capacitance of the pads and interconnections was estimated to be 1 pF to ground in all sensing pads. As can be seen, the behaviour is linear for small $C(t)/C_S$ ratios, providing a gain, for a series capacitance C_S of 68 pF, of approximately 58 mV/pF. Figure 8 shows the behaviour of the circuit with and without the parasitic cancellation circuit for different parasitic capacitances C_P. Note that the parasitic cancellation desensitizes the circuit to parasitics, thus improving the measuring capabilities of electrostatic actuators connected to the ASIC through the coaxial or triaxial cables of a probe station. In the right part of Fig. 8 the AC response of the estimator in a unity-gain configuration is shown, revealing bandwidths up to 70 MHz. However, it should be noted that when the estimator is used inside a closed-loop, like in PDOs, the phase (or delay) at a given frequency has also to be taken into account in the loop design. For the MEMS used in this work, this delay has been negligible due to the low resonant frequencies they have.

The layout of the electrostatic actuation and sensing interface is shown in Fig. 9. The circuit was implemented in the 0.35 μm AMIS $C035U$ P-Well based CMOS technology. The power consumption of the ASIC is around 25mW. In order to reduce leakage and parasitic capacitances to tolerable levels, no ESD protections on the intermediate node of the capacitive divider V_{CS} pad were implemented. Moreover, the internal routing of V_{CS} was actively shielded with the method described before.

IV. Experimental Results

The experimental measurements have been carried out using a set of MEMS devices like the one shown in Fig. 10: a two-parallel plate structure made with PolyMUMPS technology. For the device shown in Fig. 10, which will be the reference case from now on, the area of the suspended top plate is $A =$ 360x360 μm^2, the gap between the plates for $V = 0$ is $g =$ 2 μm and the pull-in voltage is around $5V$.

In order to approximately locate the main mechanical resonances of the MEMS we have followed two steps: first the simulation of the resonant modes of the mechanical structure with a finite element tool, Coventor, and second, with an impedance analyzer. The advantage of this second approach is that it allows to find accurately the location of the resonances and to study their dependence on the applied bias voltage, and on the damping of the resonator. Figure 11 presents the results of the FEM simulations of the first three modes for the reference device of Fig.10. Their respective frequencies are 16.68 kHz, 28.21 kHz and 28.22 kHz. As it can be observed, being the device symmetric, the second and third modes are in fact a $\pi/2$ rotation of one another and therefore any difference in the corresponding frequencies is due to numerical errors. In the measurements done with the impedance analyzer to accurately determine the resonant frequencies though, both modes are separated (see Figure 12), most probably due to some imperfection in the fabrication process or to residual stress.

Once the frequency response of the devices was obtained, we proceeded to build up the experimental hardware described in the previous section. In order to reduce the effects of damping losses, all measurements have been performed at low pressure conditions, using a vacuum chamber. The Q factor of the resonator for all modes is low, below 121. The bias voltage

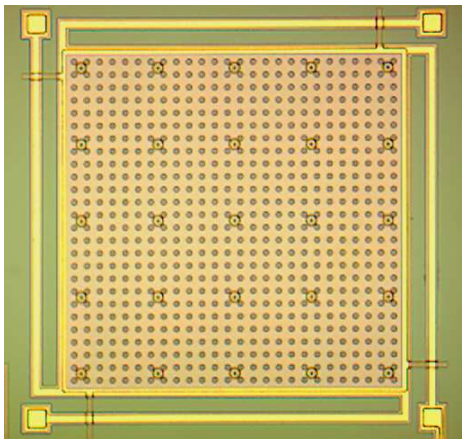

Figure 10. Top view of the MEMS device used in the experiments.

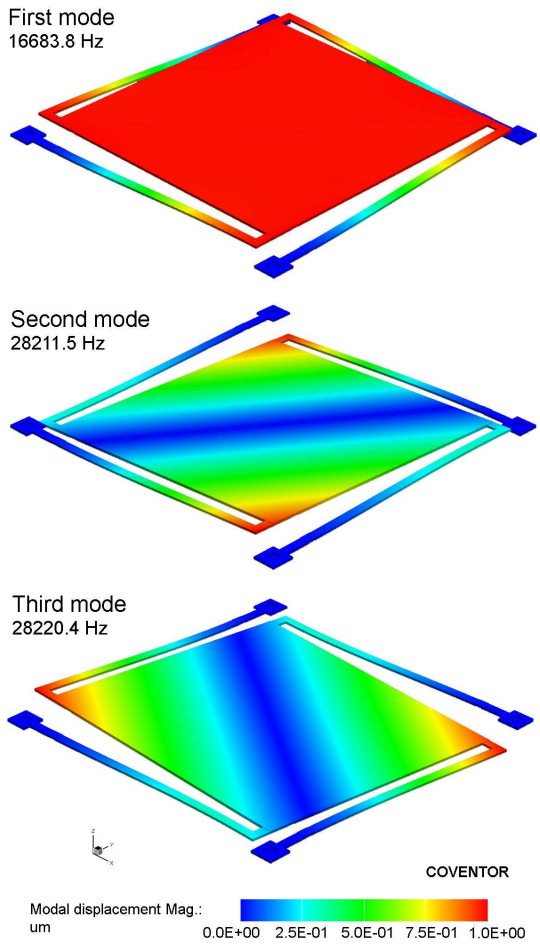

Figure 11. FEM simulations of the first three modes of the reference device of Fig. 10.

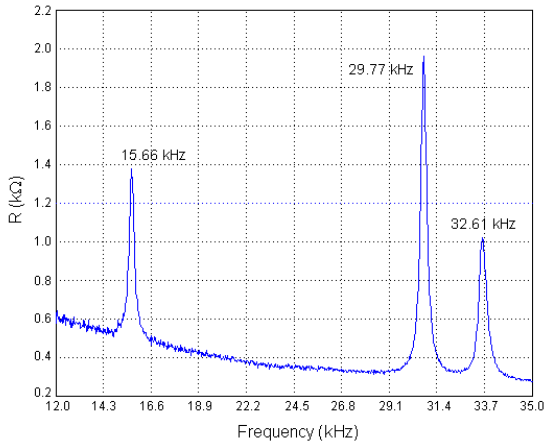

Figure 12. Real part of the impedance of the MEMS device shown in fig.10. The first three resonances can be clearly observed.

applied to the MEMS is $V_{DC} = 3V$. It must be pointed out that for low Q factors, or high damping losses, the oscillation frequency of the PDO as a function of the normalized resonant frequency becomes fractalized (the curve becomes a distorted version of the Devil's staircase fractal, formed by a succession of plateaus). This phenomenon has been reported in previous works [12].

It was found in [9], [14] that the conventional PDO allows actuating different vibrational modes of the mechanical structure simply by configuring the parameters of the feedback loop. This effect can be briefly explained as follows. Each time a delta is applied to the resonator it may increase or decrease the instantaneous velocity of the resonator. This depends on whether the instantaneous sign of the velocity of the resonator coincides with the sign of the force being applied. Since the feedback loop determines how and with what value the deltas are applied to the resonator, in average the PDO may either inject energy in the resonator or extract energy from it, until a limit cycle around the origin is reached. This will depend on the sign in the feedback loop (parameter σ in Fig. 1), the number of delay blocks in the feedback loop $(L+1)$, and the ratio between the resonant frequency of the resonator and the sampling frequency ($f = f_1/f_S$).

Therefore, given a certain resonant frequency, a sampling frequency and a feedback filter, the oscillator in average may tend to two different behaviours: a) [O] Oscillation or b) [A] Antioscillation. It has been shown that if the normalized resonant frequency, f, lies in one of the following frequency segments, depending on the value of σ:

$$\begin{aligned} \sigma = 1: &\qquad f \in \left(\frac{1+2r}{2(L+1)}, \frac{1+r}{L+1} \right), \quad r \geq 0 \\ \sigma = -1: &\qquad f \in \left(\frac{r}{L+1}, \frac{1+2r}{2(L+1)} \right), \quad r \geq 0 \end{aligned} \tag{38}$$

the oscillator will be in the Antioscillation regime, whereas if the frequency lies outside of these segments, then the PDO is in the Oscillation regime.

This means that by a suitable choice of parameters, namely L, σ and f_S, it is possible to force that a given mode is in the oscillation regime, while the others are in the antioscillation segments. Then, the PDO will generate a sustained oscillation in this specific mode. Figure 13 shows how for a certain choice of the sampling frequency, $f_S = 69.674\,kHz$, simply by changing the value of L and σ it is possible to select the first three modes of the structure. Note that for each of these combinations, only one of the resonant frequencies lies in an Oscillation segment, while the others lie in the Antioscillation regime.

Therefore, employing the selection of the parameters as discussed above and calculating the digital frequency from (35), one can distinguish between different spatial vibration modes. For the conventional PDO, this property was demonstrated in [19]. The digital frequency f_D calculated from (35) is always associated with particular mode and cannot be the same for two different vibration modes and therefore a vibration mode is uniquely defined by its digital frequency.

Although one of the most important features of PDO systems is that the oscillation frequency can be inferred from the bit stream provided by the feedback loop, in our experimental

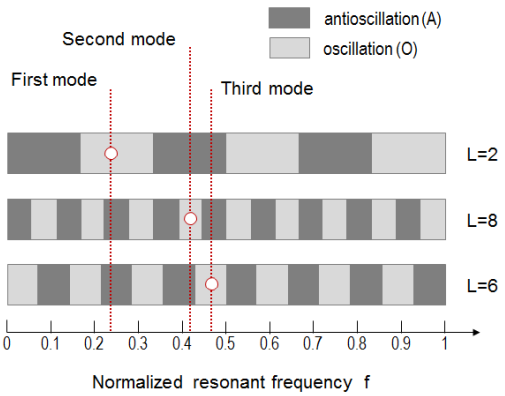

Figure 13. Oscillation and antioscillation frequency segments for the first three resonances of the reference device and three feedback filter configurations. In all cases the chosen sampling frequency is $f_S = 69.694\,kHz$. For the first and second resonances $\sigma = -1$ and for the third it is $\sigma = 1$.

measurements position waveforms provided by the ASIC were also obtained. This is not necessary, but it gives valuable additional information about the shape of the oscillations.

Thus, applying the theory associated with specific excitation of resonant modes as in the example above, we calculated the number of delays necessary to selectively excite the first three modes of the reference device at a fixed sampling frequency. The experimental results obtained for each mode are shown respectively in Figs. 14(a) to 14(c). In such figures, analog waveforms are position measurements provided by the ASIC, D1 are the reset sequences sent to the ASIC (i.e. the pulsesn applied to the resonator) and D0 is the sampling clock.

We note that, taking into account the low Q-factor of the resonators, reasonable sinusoidal waveforms are obtained for each frequency mode. Table I shows the oscillation frequencies obtained with the e-PDO, compared with the ones obtained in the FEM simulations, together with the phase noise at each mode specified at 100Hz from the carrier. Furthermore, Figure 15 shows the phase noise of the second resonance obtained with an spectrum analyzer. Since the phase noise decreases with the increase of the Q-factor [20]–[23], the phase noise of a higher-Q e-PDO should decrease.

We also remark that the waveforms obtained may exhibit brief distortion at the moments when the force pulses $V = 0$ ($b_n = 1$) are applied to the MEMS. This is clearly seen in all waveforms of Fig. 14.

Finally, it must be pointed out that the electrode configuration of the measured device is not optimal for the detection of the second and third modes, since the electrode comprises the whole area of the device. However the presented results point to the fact that if the mechanical resonance may be observed in the impedance measurement, then it should be possible to excite it by the PDO.

V. Conclusions

A new actuation scheme for electrostatic MEMS has been presented to implement the Pulsed Digital Oscillator topology. The capacitance of the device is periodically sampled, and

Figure 14. Oscilloscope screen captures showing the system behaviour at the first three resonance modes. (a) first mode at 16 kHz with $L = 2, \sigma = 1$, (b) second mode at 29.3 kHz with $L = 8, \sigma = 1$, (c) third mode at 32.39 kHz with $L = 6, \sigma = -1$. The sampling frequency is $f_s = 69.674\,kHz$ for all cases. For each mode, the waveforms shown are: MEMS position (analog channel A0), pulses applied by the PDO to the resonator, (D1) and sampling clock (D0).

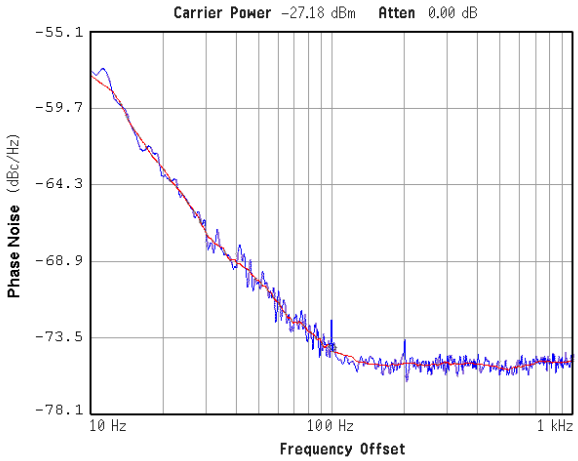

Figure 15. Phase noise obtained with the PDO exciting the second mode resonance.

Table I
FREQUENCIES OF THE FIRST THREE MODES OF THE MEMS OBTAINED WITH SIMULATIONS AND EXPERIMENTALLY WITH THE E-PDO.

Mode	Q factor	FEM Simulation [kHz]	PDO freq. analog [kHz]	PDO freq. digital	Phase noise at 100Hz [dBc/Hz]
1st	62.5	16.68	16	16.09	-56
2nd	121	28.21	29.3	29.436	-75
3rd	89	28.22	32.39	32.369	-53

the excitation consists of a bias voltage while short zero voltage pulses are applied when the PDO determines that a negative delta of force must be fed into the resonator. The control system has been theoretically analyzed and modelled with a small-signal approximation around the two voltage driving levels. An application specific integrated circuit has been designed specifically to carry out the actuation scheme. Experimental results obtained with PolyMUMPS resonators confirm that it is possible to excite different resonant modes, therefore improving the performance of the device, with this actuation scheme and the PDO oscillator topology.

VI. ACKNOWLEDGEMENTS

This work was supported in part by the Spanish Ministry of Education and Science under Projects TEC2008-06028/TEC, TEC2012-38465-C02-01, the European Social Fund (ESF) and by Science Foundation Ireland (SFI).

REFERENCES

[1] N. Yazdi, F. Ayazi, and K. Najafi, "Micromachined inertial sensors," *Proc. IEEE*, vol. 86, no. 8, pp. 1640–1659, Aug. 1998.

[2] K. B. Brown, W. Allegretto, F. E. Vermeulen, and A. M. Robinson, "Simple resonating microstructures for gas pressure measuremnets," *J. Micromechan. Microeng.*, vol. 12, pp. 204–210, 2002.

[3] G. Keskar, B. Elliott, J. Gaillard, M. J. Skove, and A. M. Rao, "Using electric actuation and detection of oscillations in microcantilevers for pressure measurements," *Sensors and Actuators A*, vol. 147, pp. 203–209, 2008.

[4] S. M. Ali, S. C. Mantell, and E. K. Longmire, "Mechanical performance of microcantilevers in liquids," *Journal of Microelectromechanical Systems*, vol. 20, no. 2, pp. 441–450, 2011.

[5] C. Hyun, J. G. Lee, and T. Kang, "Precise oscillation loop for a resonant type MEMS inertial sensors," in *SICE-ICASE, 2006. International Joint Conference*, 2006, pp. 1953–1958.

[6] E. Colinet, J. Juilard, S. Guessab, and R. Kielbasa, "Actuation of resonant MEMS using short pulsed forces," *Sensors and Actuators A: Physical*, vol. 115, pp. 118–125, 2004.

[7] M. Dominguez, J. Pons-Nin, J. Ricart, A. Bermejo, and E. Figueras-Costa, "A novel Σ-Δ pulsed digital oscillator (PDO) for MEMS," *Sensors Journal, IEEE*, vol. 5, no. 6, pp. 1379–1388, 2005.

[8] J. Ricart, J. Pons, M. Dominguez, A. Rodriguez, E. Figueras, H. M.C., J. Gutierrez, and I. Sayago, "Application of pulsed digital oscillators to volatile organic compounds sensing," *Sensors and Actuators B: Chemical*, vol. 134, no. 2, pp. 773–779, 2008.

[9] J. Ricart, J. Pons, E. Blokhina, S. Gorreta, J. Hernando, T. Manzaneque, J. Sanchez-Rojas, O. Feely, and M. Dominguez, "Control of MEMS vibration modes with pulsed digital oscillators: Part II — simulation and experimental results," *Circuits and Systems I: Regular Papers, IEEE Transactions on*, vol. 57, no. 8, pp. 1879–1890, 2010.

[10] S. Senturia, *Microsystem Design*. Kluwer Academic, 2001.

[11] S. Beeby, G. Ensell, M. Kraft, and N. White, *MEMS Mechanical Sensors*. Artech House, 2004.

[12] M. Dominguez, J. Pons-Nin, and J. Ricart, "General dynamics of pulsed digital oscillators," *Circuits and Systems I: Regular Papers, IEEE Transactions on*, vol. 55, pp. 2038–2050, 2008.

[13] A. Teplinsky and O. Feely, "Limit cycles on a MEMS oscillator," *Circuits and Systems II: Express Papers, IEEE Transactions on*, vol. 55, no. 9, pp. 882–886, 2008.

[14] E. Blokhina, J. Pons, J. Ricart, O. Feely, and M. Dominguez, "Control of MEMS vibration modes with pulsed digital oscillators: Part I — theory," *Circuits and Systems I: Regular Papers, IEEE Transactions on*, vol. 57, no. 8, pp. 1865–1878, 2010.

[15] D. Fernández, "CMOS circuits and architectures for MEMS control and signal processing," Ph.D. dissertation, Electronic Engineering Department, Technical University of Catalonia (UPC), 2008. This reference is in Spanish.

[16] R. Nadal-Guardia, A. Dehe, R. Aigner, and L. Castaner, "Current drive methods to extend the range of travel of electrostatic microactuators beyond the voltage pull-in point," *Microelectromechanical Systems, Journal of*, vol. 11, no. 3, pp. 255–263, 2002.

[17] D. Fernández, J. Madrenas, M. Domínguez, J. Pons, and J. Ricart, "Pulse drive and capacitance measurement circuit for MEMS electrostatic actuators," *Analog Integrated Circuits and Signal Processing*, vol. 57, no. 3, pp. 225–232, Dec. 2008.

[18] D. Fernández, J. Madrenas, and J. Cosp, "A self-test and dynamics characterization circuit for MEMS electrostatic actuators," *Journal of Microelectronics Reliability*, vol. 51, pp. 602–609, 2011.

[19] M. Dominguez-Pumar, E. Blokhina, J. Pons-Nin, O. Feely, and J. Sanchez-Rojas, "Pulsed digital oscillators as a tool for the selective activation of MEMS resonant modes," in *Proceedings of SPIE*, vol. 7679, 2010, p. 76792H.

[20] D. Leeson, "A simple model of feedback oscillator noise spectrum," *Proceedings of the IEEE*, vol. 54, no. 2, pp. 329–330, 1966.

[21] H. Chang, "Phase noise in self-injection-locked oscillators-theory and experiment," *Microwave Theory and Techniques, IEEE Transactions on*, vol. 51, no. 9, pp. 1994–1999, 2003.

[22] H. Chen, H. Lu, and T. Huang, "The analysis of relation between Q-factor and phase noise by using substrate-integrated waveguide cavity oscillators," in *Microwave Conference Proceedings, 2005. APMC 2005. Asia-Pacific Conference Proceedings*, vol. 4. IEEE, 2005, pp. 4–pp.

[23] S. Mahdavi, F. Nabki, M. Sawan, and M. El-Gamal, "On the testing of MEMS resonators," in *Design and Test Workshop (IDT), 2009 4th International*. IEEE, 2009, pp. 1–6.